A supramolecular nucleoside-based gel: Molecular dynamics simulation and characterization of its nanoarchitecture and self-assembly mechanism

Maria G. F. Angelerou,[†] Pim W. J. M. Frederix,[‡] Matthew Wallace,[∥] Bin Yang,[†] Alison Rodger,[§] Dave J. Adams,[⊥] Maria Marlow[†] and Mischa Zelzer,[†*]*

[†]University of Nottingham, School of Pharmacy, Nottingham, NG7 2RD, U.K.

[‡]University of Groningen, Faculty of Science and Engineering, Groningen 9747 AG, The Netherlands

[∥]University of East Anglia, School of Pharmacy, Norwich, NRT 4TJ, U.K.

[§]Macquarie University, Department of Molecular Sciences, NSW 2109, Australia

[⊥]University of Glasgow, School of Chemistry, Glasgow, G12 8QQ, U.K.

ABSTRACT Amongst the diversity of existing supramolecular hydrogels, nucleic acid-based hydrogels are of particular interest for potential drug delivery and tissue engineering applications because of their inherent biocompatibility. Hydrogel performance is directly related to nanostructure and the self-assembly mechanism of the material, an aspect that is not well understood for nucleic acid-based hydrogels in general and has not yet been explored for

cytosine based hydrogels in particular. Herein, we use a broad range of experimental characterization techniques along with molecular dynamics simulations to demonstrate the complementarity and applicability of both approaches for nucleic acid-based gelators in general and propose the self-assembly mechanism for a novel supramolecular gelator, *N4*-octanoyl-2'-deoxycytidine. The experimental data and the MD simulations are in complete agreement with each other and demonstrate the formation of a hydrophobic core within the fibrillar structures of these mainly water-containing materials. The characterization of the distinct duality of environments in this cytidine based gel will form the basis for further encapsulation of both small hydrophobic drugs and biopharmaceuticals (proteins and nucleic acids) for drug delivery and tissue engineering applications.

Introduction

In the last ten years, there has been increasing interest in supramolecular gels due to their potential applications as drug delivery systems, sensors and tissue engineering scaffolds.[1-7] Derivatives of oligopeptides[8-9] and nucleic acids i.e. nucleobases, nucleotides or nucleosides[10-11] have been extensively investigated as supramolecular gelators for biological applications due to their inherent biocompatibility. Nucleic acid-based gelators in particular are attractive because they are expected to have improved stability towards enzymatic degradation compared to peptide-based gelators.

Nucleic acid-based gels are increasingly finding their way into applications in drug delivery. They can be promising injectable delivery systems[12] of small therapeutic molecules as well as macromolecules such as proteins and nucleic acids.[4, 13-14]

For example, guanosine-based gels have been used to deliver small drug molecules in a controlled way. A 5'-deoxy-5'-iodoguanosine gel was used to release antivirals,[15] and a

guanosine-5-hydrazide gel was able to incorporate different pharmacologically active molecules including acyclovir, vitamin C and vancomycin.[16] Furthermore, thymidine-based gels have been reported in drug delivery systems for the release of macromolecules. Kaplan et al. presented a thymidine-based mechanoresponsive hydrogel for the delivery of antibodies.[13] Ramin et al. demonstrated the sustained release of both a large and a small molecule in vivo for the first time.[4] Maisani et al. have also successfully demonstrated implantation of a thymidine-based composite hydrogel as a scaffold for bone tissue engineering.[17] Notably, among the existing examples of nucleic acid-based gels, guanine and cytosine derivatives are underrepresented and poorly investigated despite their attractiveness due to the possibility to access G-quadruplexes or i-motifs, ordered structures formed specifically by guanine and cytosine-rich nucleic acid sequences, respectively, that may provide cavities to host payloads in a gel.[11]

We have recently introduced a cytosine-based gelator, a fatty acid bound to a 2'-deoxycytidine, and reported the bulk mechanical properties of the resulting gels.[18] Importantly, we also demonstrated that the mechanical properties of the gel are affected by the surface that is in contact with the gelator solution during gelation.[19] Surface-assisted self-assembly has been recognized as a largely unexplored but significant factor in self-assembly and is receiving increasing attention,[20] not least due to the implications involved when formulating gels in situ or in the presence of other components such as macromolecules or particles.

To enable rational design of a class of gelators as well as the investigation and understanding of parameters that influence self-assembly and ultimately gel properties and application, it is essential to elucidate the self-assembly mechanism. In contrast to peptide-based gelators for which the self-assembly mechanism has been extensively explored,[9, 21] a detailed, experimentally

3

supported understanding of the self-assembling mechanism of nucleic acid based gelators is lacking.

To date, evaluation of nucleic acid self-assembly typically plays an ancillary role where one or two techniques are used to investigate a specific component of the gelator. Barthélémy and co-workers reported SAXS data for an uracil based gelator indicating strongly aggregated assemblies that were observed as fibers under TEM.[22] As an organogel, the same gelator displayed repeat periods (4.6 nm) that the authors interpreted to indicate orientation of the hydrophobic part of the gelator towards the organic solvent. In a later study, Barthélémy et al. used the mismatch in fiber diameter determined by SAXS and the length of the gelator obtained by CPK modelling to propose an interdigitated organization of a thymine based gelator.[7] Iwaura et al. used XRD data of freeze dried thymine-based gels to argue that the gelator headgroup bends to expose hydroxyl groups to the outside of the fibers.[23] Temperature-dependent transmittance and CD measurements have also been used to determine the gelation temperature of thymine, adenine and uracil-based gels.[23-24] Banerjee et al. investigated the effect that different functional groups of self-assembling pyrimidine analogues can have of the final fibrillary network.[25] Roviello et al. used UV, CD and Light scattering to investigate the formation of supramolecular networks of two thymidyl dipeptides and assess their interactions with biomolecules.[26] To the best of our knowledge, no detailed investigation is currently available on the self-assembly organization or mechanism of cytosine based gelators. Moreover, while some data on other nucleic acid-based gelators exist, a comprehensive experimental and theoretical description of the contribution of all components in an amphiphilic nucleobase gelator has not yet been reported.

In this work, we systematically explore the self-assembly mechanism of the deoxycytidine derivative *N4*-octanoyl-2'-deoxycytidine. This gelator is the only member of a class of thermoresponsive cytidine-based gelators developed by our group[27] that forms a self-healing hydrogel[18] and it has been reported as a promising candidate for applications in drug delivery (e.g as depots for controlled release via gel erosion and diffusion) and tissue engineering along with the macromolecular properties of the gel (e.g. rheology).[18]

Herein, we use a range of experimental approaches to identify the contribution of the different parts of the gelator to the self-assembly process to present the first complete experimental elucidation of the self-assembled organization of a nucleic acid based gelator. Molecular dynamics (MD) simulations are ideally suited to probe the initial stages of assembly as well as the dimensions and spectroscopic properties of fully assembled nanostructures.[28-30] They have been successfully applied to monolayers and bilayers of nucleolipids and their hybridization with single-stranded DNA.[31-32] Taking advantage of this, here we further combine our experimental dataset with MD simulations to demonstrate for the first time the complementary match of experimental and theoretical data for a nucleoside gelator. This combined approach enables us to propose a detailed, comprehensive model of the self-assembly of this cytidine-based gelator and paves the way for a rational design of this class of gelators.

Results and Discussion

Gels are formed from *N4*-octanoyl-2'-deoxycytidine using a solvent mixture of 20:80% v/v ethanol:water. In the mixed solvent system used, the gelator forms a gel composed of tubular fibers (Figure S1, ESI). Whilst the gelator is able to form gels in water only[18] and does not form gels in organic solvents (e.g. methanol), the addition of ethanol in the solvent improves the

solubility of the gelator, facilitating the preparation process and gives a transparent gel ideal for spectroscopy studies.

Self-assembly induces gelator fluorescence

For gelators that contain fluorescent moieties that are involved in the self-assembly process (e.g. Fmoc- or naphthyl-conjugated peptides), fluorescence spectroscopy has been widely used to study their self-assembly processes.[8, 33-36] Unmodified nucleosides are not inherently fluorescent as shown for the example of 2'-deoxycytidine in Figure 1A. In contrast, *N4*-octanoyl-2'-deoxycytidine, the modified 2'-deoxycytidine derivative used here, displays weak fluorescence (λ_{Ex} = 326 nm, λ_{Em} = 367 nm, see Figure S2 for excitation and emission spectra) in methanol where the molecule is fully soluble (Figure 1B), suggesting fluorescence might be a useful tool to monitor self-assembly of this nucleoside gelator into structures where the aromatic moiety is protected from water.

In a mixture of 20:80% v/v ethanol:water, where *N4*-octanoyl-2'-deoxycytidine forms a supramolecular gel,[18] the intrinsic fluorescence indeed shows a marked increase compared to *N4*-octanoyl-2'-deoxycytidine in methanol and 2'-deoxycytidine in ethanol/water (Figure 1). This suggests that the self-assembled environment enhances the fluorescence of *N4*-octanoyl-2'-deoxycytidine leading to aggregation-induced emission,[5] likely due to an increase in the π-π interactions of the aromatic rings in the nucleobase that protects the molecule's fluorescent chromophore from solvent-induced quenching and leads to a strong emission at 357 nm (Figure 1B, black trace). Because of the significant difference in fluorescence intensity between the solution and the gel sample, we postulate that the increase in fluorescence intensity is more likely

to be related to the self-assembled state affecting quenching rather than any solvent-induced changes in molecular fluorescence.

To gain further understanding of the arrangement of the nucleobases in the gel, Circular dichroism (CD) experiments were performed. Aromatic nucleobase monomers are achiral molecules that become CD active due to their proximity to the chiral sugar.[37] As with double-stranded DNA, when the chiral nucleosides stack, they gain further CD intensity if the assembly is helical. As explained in detail in the ESI, circular and linear dichroism data confirmed the π-π stacking interactions of the nucleobases in the gel state.

Hydrophobic domains are formed in the gel fibers

For nucleoside-based amphiphiles, limited evidence has been provided to describe how their hydrophobic parts interact with each other. The presence of hydrophobic environments in the fibers of a cholic acid-based gel has been confirmed in the past through fluorescence by incorporating 8-anilinonaphthalene-1- sulfonic acid into the supramolecular system.[38] Nile red, a poorly water-soluble dye that dissolves and fluoresces strongly in hydrophobic environments[39] was therefore added to the gels to investigate if hydrophobic pockets are present in the self-assembled structures. After excitation of the gel containing Nile red at 540 nm, strong fluorescence at 630 nm was obtained (Figure 2A, red trace) that was absent in the control sample (Figure 2A, black trace) where a lower intensity peak at 660 nm was observed. Super resolution fluorescence microscopy showed that the fluorescence signal is spatially arranged in fiber-like structures (Figure 2B). These data clearly demonstrate the presence of a well-defined hydrophobic environment within the fiber structure.

The effect of temperature on the self-assembly

As noted above, two different fluorescence signals (the gelator's intrinsic fluorescence and the fluorescence of an incorporated dye) can be related to π-π stacking related exclusion of solvent and the association of the dye with the hydrophobic part of the gelator, respectively. By monitoring the effect of the temperature on the two different fluorescence signals, we can understand how the hydrophobic interactions contribute to the self-assembly formation and how they relate to each other.

The change in fluorescence emission intensities of the gelator itself with temperature (λ_{Ex} = 326 nm) is presented in Figure 3. The intrinsic gel fluorescence is high at room temperature, but drops drastically as the temperature increases and flattens out after 40 ˚C. Visual inspection (using the 'vial inversion test'[40]) showed that this temperature coincides with transition of the gel into a solution and confirms that the intrinsic gelator fluorescence at room temperature is related to the presence of self-assembled structures. A control experiment monitoring the change of the fluorescence signal over time at a constant temperature (ESI Figure S9) demonstrates that the differences observed in Figure 3 cannot be explained by thermal instability of the gel and are indeed related to the change in temperature. Fluorescence therefore also provides a direct route to study the behavior of the nucleobase in the self-assembly process and supports the hypothesis that during self-assembly π-π stacking of the nucleobases occurs.

The same experiment was conducted on gels containing Nile red (Figure 3; control experiment of Nile Red alone is presented in Figure S10, ESI), after excitation at two different wavelengths; 326 nm (intrinsic fluorescence from the gelator) and 540 nm (fluorescence from Nile red). There is a small shift in the transition temperature between the gel containing a dye (black trace) and

the plain gel (dashed trace) both after excitation at 326 nm, even at this low concentration of dye, suggesting that the dye is having a stabilizing effect on the gel structure. When the gels containing the dye were excited at the two different wavelengths, the data matched closely, indicating that Nile Red is interacting with the hydrophobic, aromatic part of the gelator.

NMR spectroscopy has been used extensively to elucidate supramolecular gel formation[41-43] and hence was used here to further study the effect of temperature on self-assembly. In the gel state, the resonances of the gelators are very broad due to the low mobility of the gelators in the self-assembled fibers. The assembled gelator's resonances are therefore not visible by solution-state ^{1}H NMR. Thus, the fraction of mobile gelator in solution in a sample can be determined by integration of the ^{1}H resonances of the gelator against an internal standard. This approach allows quantification of the relative amount of gelator in solution versus the amount of gelator in the assembled fibers.[43-46] In addition, saturation transfer difference (STD) NMR has been proven useful as a tool to study the exchange between assembled gelator molecules and mobile molecules in solution.[47-49] In this technique, the very broad ^{1}H resonances of the gel fibers are selectively saturated with low-power radiofrequency irradiation. Molecules in exchange with the gel fibers receive some of this saturation and therefore exhibit weaker ^{1}H NMR resonances in the ^{1}H NMR spectrum recorded immediately after saturation compared to non-saturated samples.

In Figure 4, NMR integrals and STDs of proton signals for gel samples are plotted as a function of temperature. Protons have been assigned and grouped into aromatic, aliphatic and deoxyribose (sugar) (ESI, Figure S11). STD effects are quantified as described in ESI, Figure S11 and Equation S1. A strong STD effect indicates the existence of a significant exchange between free and assembled gelator molecules.[47, 49] Between 25 ˚C and 45 ˚C, strong STD effects are observed while integration of the gelator resonances indicates that only a fraction of the

gelator molecules are NMR-visible. A significant population of the gelator is therefore aggregated at these temperatures while a degree of exchange exists between the assembled gelators and those in solution. Above 55 ˚C, no STD effects are observed and no increases in the NMR integrals with temperature relative to an internal standard are discernible. The gelators therefore have a high degree of mobility at these temperatures with no NMR-invisible assemblies present. Below 35 ˚C, the STD effects are saturated and there is no clear change with temperature.[44]

As discussed above, the gelator's fluorescence is directly related to the π-π stacking whereas the NMR data shed light into the mobility of the gelator's molecules. The discrepancy in the dissociation temperatures observed between the fluorescence (40 ˚C) and NMR (45 ˚C) may indicate that even if the π-π interactions become weaker (fluorescence data), the gelator molecules are still, to some extent, assembled (NMR data).

As the temperature increases, the NMR integrals increase until they plateau while the STD effects decrease to zero. The difference between the initial NMR integrals (at temperatures < 35 ˚C) and the integrals at higher temperatures (> 55 ˚C) is greater for the aromatic protons than the aliphatic resonances. This observation indicates that at lower temperatures (< 35 ˚C), the aromatic group has a much lower mobility in the self-assembled fibers than the alkyl chain.[50] At lower temperatures, the integrals of the deoxyribose resonances overlap slightly with those of the aliphatic tail (ESI, Figure S11), thus precluding a detailed comparison of the integrals of the deoxyribose resonances with those of the aromatic and aliphatic resonances. The alkyl chain resonances chosen for this integration did not overlap significantly with the deoxyribose resonances.

Tracking self-assembly through fluorescence properties

The fact that the fluorescence can be associated with the hydrophobic part of the molecule can give us valuable information on how the self-assembly process progresses during gel formation.[51] Tracking these two fluorescence signals (the gelator's intrinsic fluorescence and the dye's fluorescence) over time can provide a direct way to measure the gelation time and the gel's stability with time.

Gelator solutions (with and without the dye), after incubation at 60 ˚C, were directly pipetted into a cuvette and the intensity of the fluorescence was measured over time (Figure 5). For the gel (without the dye, red data), the fluorescence is of low intensity until the onset of the gel formation where the signal increases rapidly and levels off again as the gel forms. However, two small peaks are present at early time points, suggesting the formation of initial oligomers, presumably related to early stage π-π interactions.

With respect to the gel containing Nile red, we excited at two different wavelengths, 326 nm (λ_{Em} = 382 nm for the gelator's intrinsic fluorescence) and 540 nm (λ_{Em} = 625 nm for Nile red fluorescence). There is strong fluorescence emission at 2 minutes in both cases (black data at 540 nm and blue data at 326 nm), probably due to the temporary generation of localized hydrophobic environments that decreases and increases again, leveling off when the gel is fully formed at 7 minutes. This suggests a complex process of initial assembly and reorganization into stable extended structures. Even if accurate time lengths cannot be measured due to experimental limitations (there is approximately 30 seconds of uncertainty due to variations between sample preparation and starting the measurements), the three data sets almost overlay (the data where the dye is present are slightly shifted to earlier times further indicating its role in stabilizing the gels). The fact that all the data start leveling out at approximately the same time point (7 minutes) confirms that the turning point in the fluorescence traces corresponds to the time

required for gelation. Visual observations confirm the fact that the gel is formed (and becomes self-supporting within the first 10 minutes).[18] Gelation time is usually measured through rheology measurements that involves the application of strain.[9, 52] Measuring gelation time through fluorescent emission is a non-invasive way to determine gelation time in this system, that gives an advantage since no strain is applied during the gel formation so no mechanical perturbation to the structure formed.

Probing the nanostructures

To gain further insight into the local packing of the molecules after assembly, *N4*-octanoyl-2'-deoxycytidine xerogels were prepared and analyzed by X-Ray powder diffraction (Figure 6). Four main peaks can be identified. The first two sharp peaks at 2theta 5.19°/17.0 Å and 7.86°/11.2 Å (ratio 2:3) could indicate a lamellar structure with a d-spacing of 34 Å (ratio 1:2:3, suggesting the diameter of the fiber and the dimension of a single molecule at approximately 17 Å). However, data collection at lower 2theta to confirm assignment of the structures was not possible due to instrumental constraints and hence unambiguous identification of the lamellar structure was not possible. In addition to this, drying induced artefacts such as fiber aggregation could affect the results. [53]

Two broad peaks at 20.5° and 26.0° (and a shoulder at ~14.4°) dominate the spectrum in Figure 6, corresponding to spacings of 4.3 and 3.4 Å (and 6.1 Å). The gelator molecules self-assemble into loose, flexible structures, held together through π-π interactions and hydrogen bonds. Considering this, these two broad peaks are attributed to the different spacings of the nucleobases along the fiber axis, supported by different N−H−O bonds formed between the gelator molecules.

Since X-ray powder diffraction data did not conclusively allow estimation of the fiber diameter and could only be performed on dried samples, small angle neutron scattering (SANS) data for the wet gels were acquired to estimate the diameters of the fibers formed. The data were fitted to a flexible cylinder model with a polydisperse cross section. The results are presented in Figure S12, ESI. All parameters for the best fit are shown in Table S1. The fitting result indicates that the radius of the main unit of which the gel is composed is about 6.88±0.05 nm, giving a fiber diameter of approximately 14 nm. As the calculated maximum length of an individual gelator molecule (1.7 nm, see MD section below) is an order of magnitude smaller than the measured fiber diameter, it is reasonable to assume that SANS did not measure individual fibers but that the gel architecture is complex and composed of multiple fibers. Hierarchical self-assembly into structures of increasing complexity has been clearly demonstrated in the past for nucleobase-based amphiphiles. Baldelli et al. reported the self-assembly of 1,2-dilauroyl-phosphatidyl-uridine into cylindrical aggregates that under suitable conditions would form giant worm-like micelles entangled into a network.[54] Moreau et al. demonstrated how the hexagonal packing of helical structures formed by 1,2-dipalmitoyluridinophosphocholine could result in fibers.[22]

Probing the self-assembly through molecular dynamics

In order to understand the mechanism of the self-assembly on the nanoscale in more detail we performed molecular dynamics (MD) simulations of gelator molecules in 20:80% v/v ethanol:water. For the self-assembly simulations, 50 or 150 molecules of gelator were randomly placed in a small periodic box of water and ethanol (Figure 7A) and the simulations were run for 150 and 350 ns, respectively. In the low concentration simulation, gelator molecules formed

small aggregates within 5 ns, where the molecules were preferentially organized in a parallel fashion, maximizing aliphatic-aliphatic and parallel-displaced π-π contacts (Figure 7B). Note that the solvent distribution around the aggregates was not homogeneous: aliphatic tails were mainly solvated by ethanol, while the cytosine bases were mainly solvated by water, and the deoxyribose group environment was well represented by the overall solvent composition. In the final assembly ethanol was observed in the periphery of the fiber (nucleobases) but did not penetrate to the hydrophobic core. The aggregate size continuously increased by creating small micelle-like assemblies (Figure 7C). These assemblies had a transient nature, often reordering or dissociating until all molecules were in a single, flexible aggregate resembling a micelle (Figure 7D). When the concentration of the gelator molecules was tripled, a similar assembly path was observed, but it resulted in a one-dimensional assembly that stretched across the periodic boundary of the simulation box (Figure S13). This fiber or worm-like micelle still exhibited a large degree of heterogeneity though, which could be caused by the limited simulation time or the inherent flexible nature of the fibers as observed in the experiments.

To confirm the stability of the fibrous structures and also gain a better insight into the characteristics of the interactions between molecules, we designed a nanostructure by pre-ordering different numbers of gelator molecules into a fibrous structure in a chiral fashion (see Figure 8A), based on common patterns observed in the spontaneous assembly simulation. MD simulations for 150 ns revealed that flattening of the fiber was observed, but the base-base stacking and hydrogen bonding, and the tail-tail interactions remained mostly stable near the middle of the fiber (Figure 8B and 8C).

As the X-ray data represent the distances between planes of electron densities, distances obtained through the MD can be compared with the assignments of the pXRD data, as

summarized in ESI, Table S2. To compare the simulated structures to the experimental results intra-fiber distances were measured by means of radial distribution functions (RDF, ESI Figure S14). The RDF maximum representing the length of the molecule, from 5' carbon to final tail carbon, was found at 17–18 Å, in accordance with the pXRD analysis (half of the d-spacing of the suggested lamellar structure), molecules are in an extended conformation. Additionally, the diameter of the fiber, represented by a maximum in the RDF between two 5'-carbon atoms of the deoxyribose moiety, was found to be 36 Å, again indicating the SANS measurements represent bundled fibers. To give an insight into the representative distances of the intermolecular hydrogen bonds, the following distances were measured; 0.39 nm (amide C − amide N, or 0.28 nm amide O − amide N), 0.31 nm (base N(3) − amide N),   and 0.27 nm (base O(2) − amide N). These hydrogen bond distances were encountered in different frequencies as presented in ESI, Figure S15. The broad range of intermolecular hydrogen bond distances, as suggested by the pXRD data, can be supported by the different potential hydrogen bond acceptors proposed by the MD. The aromatic base stacking was found to be fairly flexible with RDF maxima at 3.6 and 5.1 Å (closest and center-center distance, respectively). Similar lengths of the molecule and distances between atoms of neighboring molecules were also found in the structures that were formed spontaneously from solvated gelator molecules, although in lower intensities because of the more pronounced heterogeneity (ESI, Figure S14). Taken together, these MD data demonstrate the spontaneous formation of fibrous nanostructures with length scales matching those obtained from experimental observations, thus confirming that the proposed fiber structures are reasonable.

Conclusions

In the present work, experimental data along with molecular dynamic simulations were used together to indicate the self-assembling mechanism and the nanoarchitecture of the fiber of a novel nucleoside (cytosine-based) gelator. The gelator molecules, driven by solvophobic forces, initially assemble into oligomeric structures then rearrange to orient themselves into a cylindrical fiber with the aliphatic chains towards the core, the nucleobases stacked together and the hydrophilic sugars towards the external surface of the fiber, whereas hydrogen bonds are stabilizing the structure. A dual environment is formed, displaying hydrophobic cores within the fiber and hydrophilic cavities surrounding them. While some structural elucidation of the self-assembly of nucleoside-based gels exist, this is the first report of the self-assembly of a cytosine based gelator. Moreover, this work demonstrates that the traditionally less well established molecular modelling of nucleobase gelators is a powerful approach to deduce information about the self-assembly of nucleic acid based gelators and matches well with experimental data.

The architecture of the present cytidine-based gel presents promising opportunities for the encapsulation of small hydrophobic molecules (e.g. anticancer drugs) as well as the stabilization of hydrophilic biopharmaceuticals (e.g. therapeutic proteins or peptides) in drug delivery applications. The ability to measure, predict and rationalize nucleobase gelator self-assembly provided by this work opens the way to a rational design of a previously unexplored class of nucleobase gelators based on cytidine for biomedical applications.

Experimental Section

Materials

2'-Deoxycytidine (lot #SLBN6031, 99% (HPLC)) and Nile Red (lot 47H3445) were purchased from Sigma Aldrich. The gelator was synthesized according to procedures reported previously.[18]

Solvents (HPLC grade) were obtained from Fischer Scientific. Analysis of the gelator was performed by NMR and LC-MS (ESI Figure S16 and S17) and purity was determined as 98% (LC-MS).

Gel preparation

In a glass container (14 cm diameter), water (300 mL) was equilibrated at 60 ˚C. The solvent mixture was prepared by mixing milliQ water and ethanol (80:20% v/v). 6.00±0.01 mg of *N4-octanoyl-2'-deoxycytidine* were pre-weighed in 1.5 ml HPLC vials. 1.2 mL of the solvent mixture was pipetted into the vials to give a 5mg/mL mixture. The vials were placed in the preheated water not in direct contact with the bottom of the container for 2 minutes. The vials were removed and mildly agitated and left to rest on the bench for 30 seconds. Consequently, the required volume for the analysis was placed in a suitable container until a transparent gel was produced.

Gels containing Nile Red

Nile Red (0.32 mg) was suspended in in premixed solvent (20:80% v/v ethanol:water, 10 mL) and sonicated for 15 minutes. The gels were prepared as above using the stock solution of Nile Red as solvent. A freshly made stock solution was prepared for each experiment.

Super resolution fluorescent microscopy

Samples were prepared according to the standard protocol, 5 µL of the warm gelator solution were pipetted onto a clean coverslip. Images were recorded with a Zeiss Elyra PS1 with a 561nm

laser: 0.1 % power100x/NA1,46 TIRF objective, with EMCCD camera in laser wide field mode, using TIRF illumination; 35 ms camera exposure time, LBF -561/642 filters.

Fluorescence spectroscopy

Spectra were recorded at a Cary Eclipse Fluorescence Spectrophotometer. The spectra were recorded with scan rate 30 nm/min, averaging time 1 sec and data interval 0.5 nm. Spectra of 14 mM 2'-deoxycytidine and *N4*-octanoyl-2'-deoxycytidine were recorded at room temperature (in premixed solvent 20:80% v/v ethanol:water and methanol) after excitation at 326 nm. The excitation slit was set at 2.5 nm and the emission slit at 5 nm.

Circular and Linear Dichroism

Samples of 2'-deoxycytidine were prepared at concentrations of 4.2 mM in methanol and ethanol:water (20:80% v/v) in 1 mm cuvette, whereas samples of *N4*-octanoyl-2'-deoxycytidine were prepared at 3.5 mM in methanol and 14 mM in ethanol: water 20:80% v/v in 1 mm cuvette and 0.1 mm demountable cuvette, respectively. Circular and linear dichroism spectra were recorded simultaneously at a Jasco J-815 instrument. The acquisition parameters were; bandwidth 2 nm, data pitch 0.2 nm, scanning speed 100nm/min and each spectrum was the product of averaging 4 accumulations.

Fluorescence temperature experiment

Spectra of the gels (5 mg/mL in premixed solvent 20:80% v/v ethanol:water) were recorded at 25, 30, 35, 40, 45, 50, 55, 60, 65 and 70 ˚C, with 326 nm excitation and 382 nm emission wavelengths. The excitation slit was set at 2.5 nm and the emission slit at 5 nm. Temperature

experiments of the gels after the incorporation of the Nile Red (5 mg/mL in premixed stock solution 20:80% v/v ethanol:water) were recorded at same temperatures as before with 540 nm excitation and 625 nm emission wavelengths. The excitation slit was set at 5 nm and the emission slit at 5 nm.

An excitation spectrum was recorded for the gels (5 mg/mL in premixed solvent 20:80% v/v ethanol:water) and the emission wavelength was set at 382 nm. The excitation slit was set at 2.5 nm and the emission slit at 5 nm.

Kinetics experiment

The gel was prepared according to the standard protocol and immediately transferred into the sample holder to record the fluorescent spectrum. Data points were collected for 40 minutes. For the gel, the excitation slit was set at 2.5 nm and the emission slit at 5 nm, the excitation wavelength was 326 nm and the emission 382 nm. For the gel after the incorporation of the Nile Red, the excitation slit was set at 5 nm and the emission slit at 5 nm, the excitation wavelength was 540 nm and the emission 625 nm, averaging time 0.0125 ns.

Powder X-ray Diffraction

Gels were prepared according to the general preparation method mentioned before and left to fully dry at room temperature. Powder X-ray diffraction (pXRD) patterns on the dry gel were collected over the 2theta range of 3-40o on a PANalytical X'pert diffractometer using Cu-Kα1 radiation (λ=1.5406Å).

Molecular dynamics simulations

Molecular dynamics simulations were performed using the GROMACS 4.6.7 package.[55] Force field parameters for the cytidine derivative were based on a combination of the 2'-deoxycytidine and aliphatic tail parameters of the GROMOS54a8 force field.[56-57] After a short energy minimization, simulations of a pre-ordered fiber (50 ns) or 50/150 randomly dispersed amphiphiles (150 ns) in a periodic box of 10 x 10 x 10 nm filled with a pre-equilibrated SPC water / ethanol mixture[58] were run in the NPT ensemble with time steps of 1 fs. Bonds involving hydrogens were constrained using the LINCS algorithm, [59] except from water bonds which were constrained using the more efficient SETTLE algorithm. [60-61] Center of mass motion of the system was removed every 100 steps. Temperature was kept at 298 K using the velocity-rescaling thermostat[61] (τT= 1.0 ps) and pressure at 1.0 bar using the Berendsen barostat[62] (τp= 1.5 ps). Van der Waals and electrostatic forces were cut off at 1.4 nm using the Verlet list scheme; long-range electrostatic interaction were treated using a Barker-Watts reaction field with $\varepsilon RF = 62$. Visualisation of the simulations was done using the VMD program v. 1.9.3.[63] Radial distribution functions were calculated on the final one-third of the simulations using the GROMACS package with a bin width of 0.002 (see ESI for further details).

NMR experiment

To prepare a sample for analysis by NMR spectroscopy, 4 mg of N4-octanoyl-2'-deoxycytidine was weighed into a 1.2 mL HPLC vial. A solution of 80% D_2O/20% ethanol-d6 was then added to the vial to create a 5 mg/mL mixture of *N4*-octanoyl-2'-deoxycytidine. The vial was then placed in a water bath at 60 ˚C for 2 minutes, whereupon the vial was removed from the bath, gently shaken and stood for 30 seconds. The solution was then injected into a pre-heated 5 mm NMR tube using a preheated 1 mL polypropylene syringe fitted with a 200 µL

polypropylene pipette tip. The NMR tube had been preheated by placing it in the water bath. The syringe was preheated by placing it in a 10 mm NMR tube which was immersed in the bath. A 2 mm (O.D) capillary (New Era Enterprises, New Jersey, USA) containing 20 mM 3-(trimethylsilyl)propionic-2,2,3,3-d4 acid sodium salt (TSP) in D_2O was then inserted into the sample when still liquid. A clear gel formed in the tube within 10 minutes. After 1 hour had elapsed, the sample was transferred to the spectrometer for analysis.

NMR experiments were performed on a Bruker Avance II 400 MHz wide bore spectrometer operating at 400.20 MHz for ^{1}H. TSP (0 ppm) was used a reference for all spectra. The sample was heated in 5 ˚C increments, with a seven minute equilibration time at each temperature prior to acquiring NMR data. ^{1}H integrals were measured from spectra obtained in 4 scans using a 30˚ excitation pulse, a relaxation delay of 40 s and a signal acquisition time of 4 s. The total acquisition time was 2 minutes and 56 seconds. STD spectra were acquired using a 90˚ excitation pulse and a signal acquisition time of 4 seconds. The relaxation delay was set at 8.1 s with presaturation applied during the last second at -5 ppm (on resonance) and at -250 ppm (off resonance). Presaturation was delivered using twenty Gaussian pulses of 50 ms duration and peak powers of 380 Hz. The separation between the pulses was 1 ms. On and off-resonance spectra were acquired alternately in 4 scans at each frequency. 8 dummy scans were acquired prior to signal acquisition. The total acquisition time for STD spectra was thus 3 minutes 16 seconds.
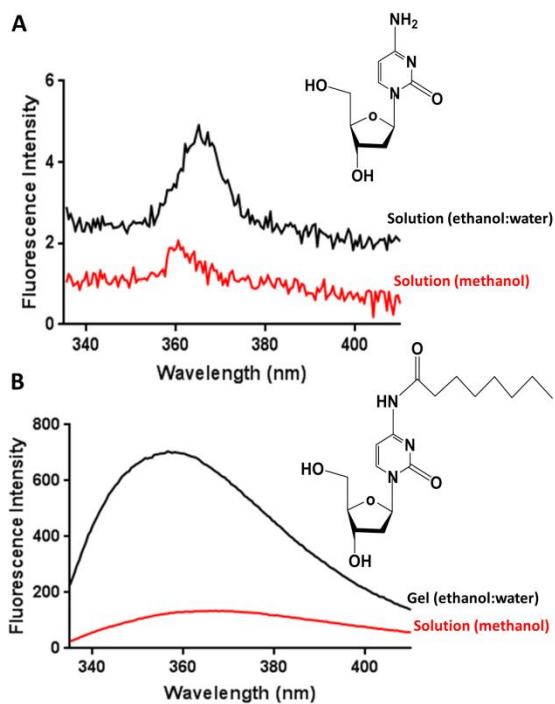
FIGURE 1. Fluorescence emission spectra of (A) 2'-deoxycytidine and (B) *N4*-octanoyl-2'-deoxycytidine at a concentration of 14 mM in either 20:80% v/v ethanol:water (black trace) or methanol (red trace) upon excitation at 326 nm.
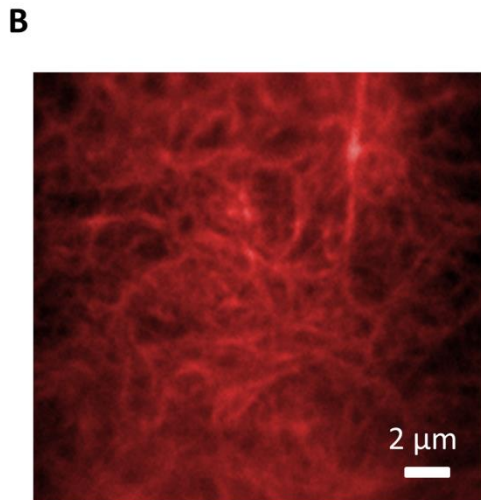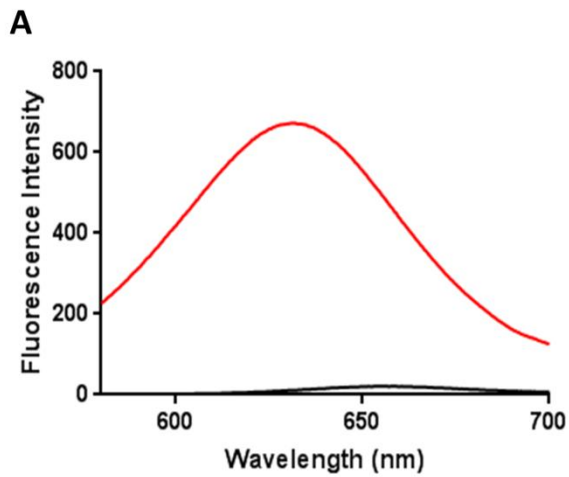
FIGURE 2. (A) Fluorescence emission spectra (λ_{Ex} = 540 nm) of Nile Red (approximately 0.1 mM) in ethanol:water (20:80% v/v) (black trace) and the gel after the incorporation of Nile Red in ethanol:water (red trace). (B) Super Resolution Fluorescence Microscopy image of gels after the incorporation of Nile Red.
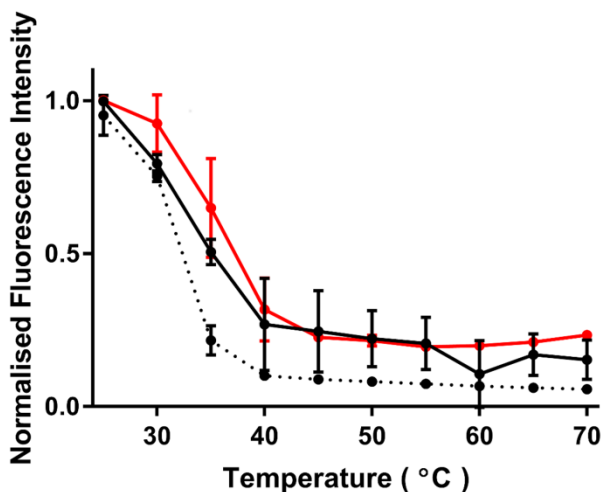
FIGURE 3. Temperature dependent change in fluorescence emission intensities of *N4*-octanoyl-2'-deoxycytidine gelator during the gel-sol transition (heating up from 25 to 70 ˚C). Gels in ethanol:water (20:80% v/v) after excitation at 326 nm and emission at 382 nm (inherent gelator fluorescence, dashed trace) and gels after the incorporation of Nile Red in ethanol:water (20:80% v/v) after excitation at 540 nm and emission at 625 nm (Nile Red fluorescence, red trace) and after excitation at 326 nm and emission at 360 nm (inherent fluorescence in presence of Nile Red, black trace). The intensities were normalised to the highest observed value in each condition. The bars represent the standard deviations (number of repeats N=3).
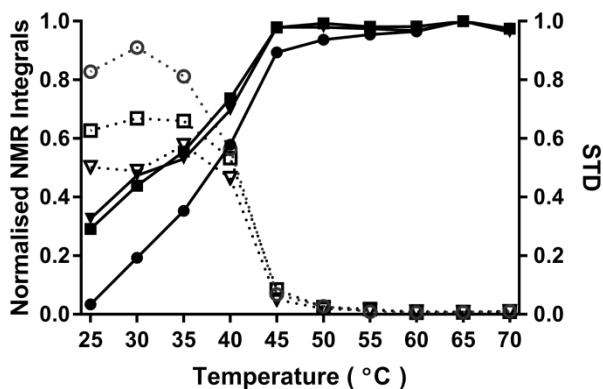
FIGURE 4. Plots of ^{1}H NMR integrals measured on *N4*-octanoyl-2'-deoxycytidine gels against temperature. STDs are also plotted (dashed traces). Trimethylsilylpropanoic acid (TSP) was used as the reference for integration. Different groups of the gelator's protons are presented; aromatic (circles), deoxyribose (triangles) and aliphatic (squares).
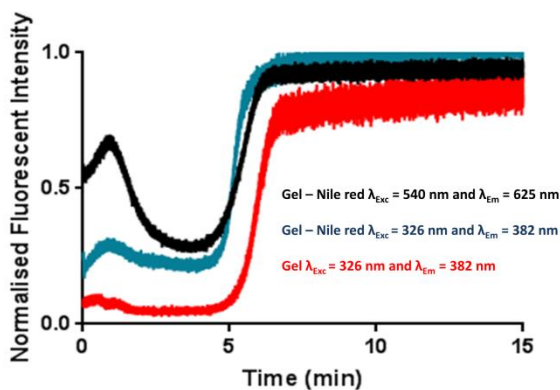

FIGURE 5. Gel formation; normalized fluorescence emis-sion intensity vs time during gel formation (cooling down process from 60 ˚C to 25 ˚C). Fluorescence of gels in ethanol:water (20:80% v/v) upon excitation at 326 nm and emission at 382 nm (with (blue trace) and without nile red (red trace)) and fluorescence of gels after the incorporation of Nile Red in ethanol:water

upon excitation at 540 nm and emission at 625 nm (black trace). The intensities were normalized to the highest observed value.
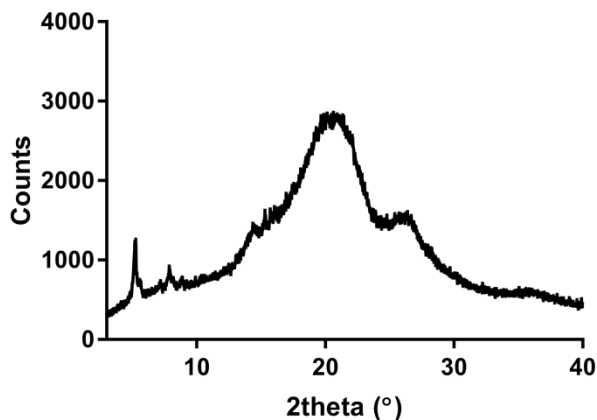

FIGURE 6. Powder X-Ray diffraction data obtained from xerogels of *N4*-octanoyl-2'-deoxycytidine.
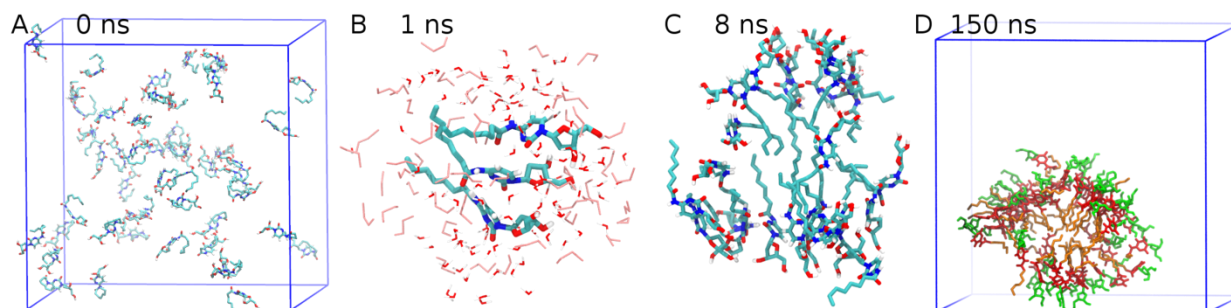

FIGURE 7. Snapshots from an MD simulation of the self-assembly of 50 gelator molecules in ethanol:water. (A) Starting point of randomly dispersed gelator molecules. Periodic boundary conditions are indicated by the blue cube. Solvent is omitted for clarity. (B) From 0-5 ns, small aggregates of parallel-aligned gelator molecules were observed. Note that the hydrophobic tail is preferentially solvated by ethanol (pink), while the polar nucleobases are stacking and solvated by water. (C) Transient micellar structures are observed from 5-150 ns. (D) Endpoint of a 150 ns

simulation displaying a micellar assembly. Green: deoxyribose red: nucleobase, orange: aliphatic tail.
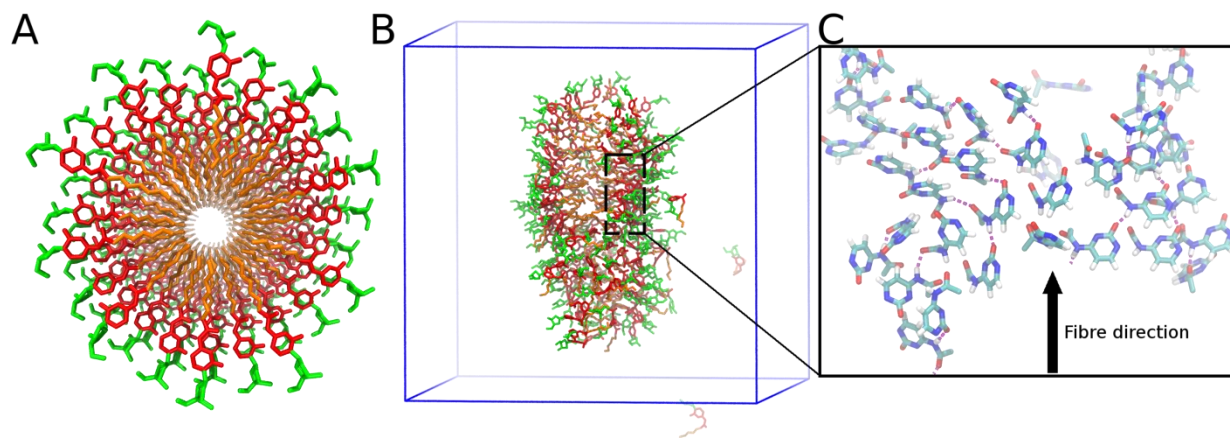

Figure 8. Snapshots from an MD simulation of 160 pre-ordered gelator molecules in ethanol:water. (A) Chiral starting structure. Green: pentose, red: nucleobase, orange: aliphatic tail. (B) Final structure after 50 ns. Periodic boundary conditions are indicated by the blue cube. Solvent is omitted for clarity. (C) Expansion of only the cytosine bases in the fiber indicating H-bonding (in purple) and parallel-displaced π-π-stacking.

ASSOCIATED CONTENT

This material is available free of charge via the Internet at http://pubs.acs.org. AFM and TEM images of the gel showing the nanoarchitecture, analysis of the fluorescence properties of the gelator, Circular and linear dichroism data of the gel formation, investigations of the variability in the molecular arrangement of the stacked nucleobases, the effect of temperature over time in the self-assembly, additional information of the SANS data and the molecular modelling data as well as structural characterization of the gelator.

AUTHOR INFORMATION

Corresponding Author

* E-mail: pazmem@exmail.nottingham.ac.uk; pazmz@exmail.nottingham.ac.uk

Author Contributions

The manuscript was written through contributions of all authors. MGFA, PWJMF, MW, BY have conducted the experimental work. MZ, MM, AR, DA have contributed to the design, data interpretation and preparation of the manuscript. All authors have given approval to the final version of the manuscript.

REFERENCES

1.   Adler-Abramovich, L.; Gazit, E., The physical properties of supramolecular peptide assemblies: from building block association to technological applications. *Chem. Soc. Rev.* **2014,** *43* (20), 6881-6893.
2.   Busseron, E.; Ruff, Y.; Moulin, E.; Giuseppone, N., Supramolecular self-assemblies as functional nanomaterials. *Nanoscale* **2013,** *5* (16), 7098-7140.
3.   Skilling, K. J.; Citossi, F.; Bradshaw, T. D.; Ashford, M.; Kellam, B.; Marlow, M., Insights into low molecular mass organic gelators: a focus on drug delivery and tissue engineering applications. *Soft Matter* **2014,** *10* (2), 237-256.
4.   Ramin, M. A.; Sindhu, K. R.; Appavoo, A.; Oumzil, K.; Grinstaff, M. W.; Chassande, O.; Barthélémy, P., Cation Tuning of Supramolecular Gel Properties: A New Paradigm for Sustained Drug Delivery. *Advanced Materials* **2017,** *29* (13).
5.   Nuthanakanti, A.; Srivatsan, S. G., Hierarchical self-assembly of switchable nucleolipid supramolecular gels based on environmentally-sensitive fluorescent nucleoside analogs. *Nanoscale* **2016,** *8* (6), 3607-3619.
6.   Nuthanakanti, A.; Srivatsan, S. G., Surface-tuned and metal ion-responsive supramolecular gels based on nucleolipids. *ACS Applied Materials & Interfaces* **2017**.
7.   Godeau, G.; Bernard, J.; Staedel, C.; Barthélémy, P., Glycosyl–nucleoside–lipid based supramolecular assembly as a nanostructured material with nucleic acid delivery capabilities. *Chemical Communications* **2009,** (34), 5127-5129.
8.   Johnson, E. K.; Adams, D. J.; Cameron, P. J., Peptide based low molecular weight gelators. *Journal of Materials Chemistry* **2011,** *21* (7), 2024-2027.
9.   Chen, L.; Morris, K.; Laybourn, A.; Elias, D.; Hicks, M. R.; Rodger, A.; Serpell, L.; Adams, D. J., Self-assembly mechanism for a naphthalene− dipeptide leading to hydrogelation. *Langmuir* **2009,** *26* (7), 5232-5242.
10.   Peters, G. M.; Davis, J. T., Supramolecular gels made from nucleobase, nucleoside and nucleotide analogs. *Chemical Society Reviews* **2016,** *45* (11), 3188-3206.
11.   Baillet, J.; Desvergnes, V.; Hamoud, A.; Latxague, L.; Barthélémy, P., Lipid and Nucleic Acid Chemistries: Combining the Best of Both Worlds to Construct Advanced Biomaterials. *Advanced Materials* **2018**.
12.   Ramin, M. A.; Latxague, L.; Sindhu, K. R.; Chassande, O.; Barthélémy, P., Low molecular weight hydrogels derived from urea based-bolaamphiphiles as new injectable biomaterials. *Biomaterials* **2017,** *145*, 72-80.
13.   Kaplan, J.; Barthélémy, P.; Grinstaff, M., Self-assembled nanofiber hydrogels for mechanoresponsive therapeutic anti-TNFα antibody delivery. *Chemical Communications* **2016,** *52* (34), 5860-5863.
14.   Allain, V.; Bourgaux, C.; Couvreur, P., Self-assembled nucleolipids: from supramolecular structure to soft nucleic acid and drug delivery devices. *Nucleic acids research* **2011,** *40* (5), 1891-1903.

15.   Plank, T. N.; Davis, J. T., AG 4· K+ hydrogel that self-destructs. *Chemical Communications* **2016,** *52* (28), 5037-5040.

16.   Sreenivasachary, N.; Lehn, J. M., Structural Selection in G-Quartet-Based Hydrogels and Controlled Release of Bioactive Molecules. *Chemistry–An Asian Journal* **2008,** *3* (1), 134-139.

17.   Maisani, M.; Ziane, S.; Ehret, C.; Levesque, L.; Siadous, R.; Le Meins, J. F.; Chevallier, P.; Barthélémy, P.; De Oliveira, H.; Amédée, J., A new composite hydrogel combining the biological properties of collagen with the mechanical properties of a supramolecular scaffold for bone tissue engineering. *Journal of tissue engineering and regenerative medicine* **2017**.

18.   Skilling, K. J.; Kellam, B.; Ashford, M.; Bradshaw, T. D.; Marlow, M., Developing a self-healing supramolecular nucleoside hydrogel. *Soft Matter* **2016,** *12* (43), 8950-8957.

19.   Angelerou, M. G. F.; Sabri, A.; Creasey, R.; Angelerou, P.; Marlow, M.; Zelzer, M., Surface-directed modulation of supramolecular gel properties. *Chemical Communications* **2016,** *52* (23), 4298-4300.

20.   Schaaf, P.; Vigier-Carrière, C.; Boulmedais, F.; Jierry, L., Surface-assisted self-assembly strategies leading to supramolecular hydrogels. *Angewandte Chemie* **2017**.

21.   Smith, A. M.; Williams, R. J.; Tang, C.; Coppo, P.; Collins, R. F.; Turner, M. L.; Saiani, A.; Ulijn, R. V., Fmoc-Diphenylalanine Self Assembles to a Hydrogel via a Novel Architecture Based on π–π Interlocked β-Sheets. *Advanced Materials* **2008,** *20* (1), 37-41.

22.   Moreau, L.; Barthélémy, P.; El Maataoui, M.; Grinstaff, M. W., Supramolecular assemblies of nucleoside phosphocholine amphiphiles. *Journal of the American Chemical Society* **2004,** *126* (24), 7533-7539.

23.   Iwaura, R.; Yoshida, K.; Masuda, M.; Yase, K.; Shimizu, T., Spontaneous fiber formation and hydrogelation of nucleotide bolaamphiphiles. *Chemistry of materials* **2002,** *14* (7), 3047-3053.

24.   Bogliotti, N.; Ritter, A.; Hebbe, S.; Vasella, A., Oligonucleotide Analogues with Integrated Bases and Backbones. Part 19. *Helvetica chimica acta* **2008,** *91* (11), 2181-2202.

25.   Banerjee, P.; Pyne, A.; Pal, S.; Karan, C. K.; Sarkar, N., Self-assembling behavior of pyrimidine analogues: Unveiling the factors behind morphological diversity. *Journal of colloid and interface science* **2018,** *522*, 63-73.

26.   Roviello, G. N.; Oliviero, G.; Di Napoli, A.; Borbone, N.; Piccialli, G., Synthesis, self-assembly-behavior and biomolecular recognition properties of thyminyl dipeptides. *Arabian Journal of Chemistry* **2018**.

27.   Skilling, K. J.; Ndungu, A.; Kellam, B.; Ashford, M.; Bradshaw, T. D.; Marlow, M., Gelation properties of self-assembling N-acyl modified cytidine derivatives. *Journal of Materials Chemistry B* **2014,** *2* (47), 8412-8417.

28.   Thota, N.; Jiang, J., Computational amphiphilic materials for drug delivery. *Frontiers in Materials* **2015,** *2*, 64.

29.   Manandhar, A.; Kang, M.; Chakraborty, K.; Tang, P. K.; Loverde, S. M., Molecular simulations of peptide amphiphiles. *Organic & biomolecular chemistry* **2017,** *15* (38), 7993-8005.

30.   Yuan, C.; Li, S.; Zou, Q.; Ren, Y.; Yan, X., Multiscale simulations for understanding the evolution and mechanism of hierarchical peptide self-assembly. *Physical Chemistry Chemical Physics* **2017,** *19* (35), 23614-23631.

31.   Pan, D.; Tang, C.; Fan, X.; Li, Y.; Yang, X.; Jin, H.; Guan, Z.; Yang, Z.; Zhang, L., Thymidine-based amphiphiles and their bonding to DNA. *New Journal of Chemistry* **2013,** *37* (4), 1122-1127.

32.   Lepeltier, E.; Bourgaux, C.; Rosilio, V. r.; Poupaert, J. H.; Meneau, F.; Zouhiri, F.; Lepêtre-Mouelhi, S.; Desmaële, D.; Couvreur, P., Self-assembly of squalene-based nucleolipids: relating the chemical structure of the bioconjugates to the architecture of the nanoparticles. *Langmuir* **2013,** *29* (48), 14795-14803.

33.   Raeburn, J.; Adams, D. J., Multicomponent low molecular weight gelators. *Chemical Communications* **2015,** *51* (25), 5170-5180.

34.   Du, X.; Zhou, J.; Shi, J.; Xu, B., Supramolecular hydrogelators and hydrogels: from soft matter to molecular biomaterials. *Chem. Rev* **2015,** *115* (24), 13165-13307.

35.   Fichman, G.; Gazit, E., Self-assembly of short peptides to form hydrogels: Design of building blocks, physical properties and technological applications. *Acta biomaterialia* **2014,** *10* (4), 1671-1682.

36.   Hughes, M.; Birchall, L. S.; Zuberi, K.; Aitken, L. A.; Debnath, S.; Javid, N.; Ulijn, R. V., Differential supramolecular organisation of Fmoc-dipeptides with hydrophilic terminal amino acid residues by biocatalytic self-assembly. *Soft Matter* **2012,** *8* (45), 11565-11574.

37.   Nordén, B.; Rodger, A.; Dafforn, T., *Linear dichroism and circular dichroism*. The Royal Society of Chemistry: 2010.

38.   Maitra, U.; Mukhopadhyay, S.; Sarkar, A.; Rao, P.; Indi, S., Hydrophobic pockets in a nonpolymeric aqueous gel: observation of such a gelation process by color change. *Angewandte Chemie International Edition* **2001,** *40* (12), 2281-2283.

39.   Greenspan, P.; Mayer, E. P.; Fowler, S. D., Nile red: a selective fluorescent stain for intracellular lipid droplets. *The Journal of cell biology* **1985,** *100* (3), 965-973.

40.   Gels, M., Materials with self-assembled fibrillar networks, ed. RG Weiss and P. Terech. Springer, Dordrecht: 2006.

41.   Morris, K. L.; Chen, L.; Raeburn, J.; Sellick, O. R.; Cotanda, P.; Paul, A.; Griffiths, P. C.; King, S. M.; O'Reilly, R. K.; Serpell, L. C., Chemically programmed self-sorting of gelator networks. *Nature communications* **2013,** *4*, 1480.

42.   Escuder, B.; LLusar, M.; Miravet, J. F., Insight on the NMR study of supramolecular gels and its application to monitor molecular recognition on self-assembled fibers. *The Journal of organic chemistry* **2006,** *71* (20), 7747-7752.

43.   Hirst, A. R.; Coates, I. A.; Boucheteau, T. R.; Miravet, J. F.; Escuder, B.; Castelletto, V.; Hamley, I. W.; Smith, D. K., Low-molecular-weight gelators: elucidating the principles of gelation based on gelator solubility and a cooperative self-assembly model. *Journal of the American Chemical Society* **2008,** *130* (28), 9113-9121.

44.   Angulo, J.; Enríquez-Navas, P. M.; Nieto, P. M., Ligand–receptor binding affinities from saturation transfer difference (STD) NMR spectroscopy: the binding isotherm of STD initial growth rates. *Chemistry-A European Journal* **2010,** *16* (26), 7803-7812.

45.   Šaman, D.; Kolehmainen, E., Studies on supramolecular gel formation using DOSY NMR. *Magnetic Resonance in Chemistry* **2015,** *53* (4), 256-260.

46.   Duncan, D. C.; Whitten, D. G., 1H NMR Investigation of the Composition, Structure, and Dynamics of Cholesterol− Stilbene Tethered Dyad Organogels. *Langmuir* **2000,** *16* (16), 6445-6452.

47.   Ramalhete, S. M.; Nartowski, K. P.; Sarathchandra, N.; Foster, J. S.; Round, A. N.; Angulo, J.; Lloyd, G. O.; Khimyak, Y. Z., Supramolecular amino acid based hydrogels: probing the contribution of additive molecules using NMR spectroscopy. *Chemistry-A European Journal* **2017,** *23* (33), 8014-8024.

48. Segarra-Maset, M. D.; Escuder, B.; Miravet, J. F., Selective Interaction of Dopamine with the Self-Assembled Fibrillar Network of a Molecular Hydrogel Revealed by STD-NMR. *Chemistry-A European Journal* **2015,** *21* (40), 13925-13929.

49. Wallace, M.; Iggo, J. A.; Adams, D. J., Probing the surface chemistry of self-assembled peptide hydrogels using solution-state NMR spectroscopy. *Soft matter* **2017,** *13* (8), 1716-1727.

50. Iqbal, S.; Rodríguez-LLansola, F.; Escuder, B.; Miravet, J. F.; Verbruggen, I.; Willem, R., HRMAS 1H NMR as a tool for the study of supramolecular gels. *Soft Matter* **2010,** *6* (9), 1875-1878.

51. Raeburn, J.; Chen, L.; Awhida, S.; Deller, R. C.; Vatish, M.; Gibson, M. I.; Adams, D. J., Using molecular rotors to probe gelation. *Soft Matter* **2015,** *11* (18), 3706-3713.

52. Ryan, D. M.; Anderson, S. B.; Senguen, F. T.; Youngman, R. E.; Nilsson, B. L., Self-assembly and hydrogelation promoted by F 5-phenylalanine. *Soft Matter* **2010,** *6* (3), 475-479.

53. Mears, L. L.; Draper, E. R.; Castilla, A. M.; Su, H.; Dietrich, B.; Nolan, M. C.; Smith, G. N.; Doutch, J.; Rogers, S.; Akhtar, R., Drying affects the fiber network in low molecular weight hydrogels. *Biomacromolecules* **2017,** *18* (11), 3531-3540.

54. Baldelli Bombelli, F.; Berti, D.; Keiderling, U.; Baglioni, P., Giant polymerlike micelles formed by nucleoside-functionalized lipids. *The Journal of Physical Chemistry B* **2002,** *106* (44), 11613-11621.

55. Hess, B.; Kutzner, C.; Van Der Spoel, D.; Lindahl, E., GROMACS 4: algorithms for highly efficient, load-balanced, and scalable molecular simulation. *Journal of chemical theory and computation* **2008,** *4* (3), 435-447.

56. Reif, M. M.; Hünenberger, P. H.; Oostenbrink, C., New interaction parameters for charged amino acid side chains in the GROMOS force field. *Journal of chemical theory and computation* **2012,** *8* (10), 3705-3723.

57. Reif, M. M.; Winger, M.; Oostenbrink, C., Testing of the GROMOS force-field parameter set 54A8: structural properties of electrolyte solutions, lipid bilayers, and proteins. *Journal of chemical theory and computation* **2013,** *9* (2), 1247-1264.

58. Berendsen, H. J.; Postma, J. P.; van Gunsteren, W. F.; Hermans, J., Interaction models for water in relation to protein hydration. In *Intermolecular forces*, Springer: 1981; pp 331-342.

59. Hess, B., P-LINCS: A parallel linear constraint solver for molecular simulation. *Journal of Chemical Theory and Computation* **2008,** *4* (1), 116-122.

60. Miyamoto, S.; Kollman, P. A., SETTLE: an analytical version of the SHAKE and RATTLE algorithm for rigid water models. *Journal of computational chemistry* **1992,** *13* (8), 952-962.

61. Bussi, G.; Donadio, D.; Parrinello, M., Canonical sampling through velocity rescaling. *The Journal of chemical physics* **2007,** *126* (1), 014101.

62. Berendsen, H. J.; Postma, J. v.; van Gunsteren, W. F.; DiNola, A.; Haak, J., Molecular dynamics with coupling to an external bath. *The Journal of chemical physics* **1984,** *81* (8), 3684-3690.

63. Humphrey, W.; Dalke, A.; Schulten, K., VMD: Visual Molecular Dynamics. *Journal of Molecular Graphics* **1996,** *14* (1), 33-38.